Journal of Marine Research, 54, 55–72, 1996

The flow field off southwest India at 8N during the southwest monsoon of August 1993

by Lothar Stramma[1], Jürgen Fischer[1] and Friedrich Schott[1]

ABSTRACT

The flow field off the southwest coast of India at 8N was investigated during RV *Sonne* cruise 89 in August 1993 by direct velocity observations from shipboard- and lowered-ADCP and geostrophic computations from CTD stations. The upper ocean between 75E and 76°52′E near the South Indian shelf was governed by a northward flow with a subsurface velocity maximum of 25 cm s^{-1} at about 100 m depth. This flow, organized as a poleward undercurrent hugging the continental slope, is typical for the southwest monsoon season. The northward transport in August 1993 was 4.7 Sv (1 Sverdrup = 10^6 m^3 s^{-1}) for the upper 300 m from the shipboard ADCP. Earlier geostrophic observations showed southward surface flow above the poleward undercurrent, but in August 1993 the northward flow reached to the surface and in the geostrophy calculations, i.e. without the southward Ekman flow near the surface, there was even no clear subsurface core. The *T-S* characteristics show that Bay of Bengal Water (BBW) was carried with this flow, and low wind conditions seemed to be connected to the flow of BBW from the southern tip of Sri Lanka toward the southwest coast of India.

Further offshore, two meridional current bands were identified in the upper 300 m of the ocean. West of the coastal undercurrent a band of southward flow existed with velocities up to 35 cm s^{-1} above and to the east of the Chagos-Laccadive Ridge, from 72°10′E to 75E. The associated geostrophic transport in the upper 500 m was 5.2 Sv. As the *T-S* relation was different from that of the northward flow, this current band was not a local recirculation of the poleward undercurrent. Further west, the flow was weak, but intensified toward the central Arabian Sea, between 66E and 69°20′E, where another southward current band was found with velocities of up to 20 cm s^{-1} and a total geostrophic transport for the upper 300 m of −7.2 Sv.

1. Introduction

Off the southwest coast of India (Kerala coast), the surface currents are toward the equator and the thermocline shallows near the coast during the southwest (northern summer) monsoon (Shetye *et al.,* 1990). During the northeast monsoon in northern winter the surface currents are northward and the thermocline deepens near the coast (Shetye *et al.,* 1991). The mixed-layer depth near southwest India changes from 80 m in January to 30 m in September (Rao *et al.,* 1989). Associated with the monsoons is also a complete reversal of the subsurface coastal circulation

1. Institut für Meereskunde, an der Universität Kiel, Düsternbrooker Weg 20, 24105 Kiel, Germany.

(Naqvi *et al.,* 1990). During the southwest monsoon a northward undercurrent appears to carry low nitrite and relatively well-oxygenated waters off the Indian continental margin. This feature is absent during the northeast monsoon. Just west of the Laccadive Ridge an anticyclonic eddy forms during December to April centered at 10N, 70E, but it translates westward by January with a subsequent dissipation in midbasin (Bruce *et al.,* 1994), and this eddy is not present during the southwest monsoon.

The hydrography and circulation off the west coast of India at the eastern boundary of the Arabian Sea was investigated during the southwest monsoon of 1987 by Shetye *et al.* (1990). South of 15N they observed upwelling near the coast and a shallow (approximately 75 to 100 m deep) equatorward surface current, below which there were signatures of downwelling indicative of a poleward undercurrent hugging the continental slope. The undercurrent carried low salinity water which according to Shetye *et al.* (1990) originated in the southwestern Bay of Bengal. Near the coast at 8N, the upper ocean hydrography was characterized by upward displaced isotherms and an approximately 100 m deep and 150 km wide equatorward flow (Shetye *et al.,* 1990). Below this lies a northward undercurrent, approximately 40 km wide, with its core identifiable by a salinity minimum at about 150 m depths. The transport of the equatorward surface current was estimated at 4 Sv (1 Sverdrup = 10^6 m^3 s^{-1}) south of 10N, where eastward flow through the Nine-Degree Channel joined the southward current. Southward motion along the southwest coast of India and possibly along the west coast of Sri Lanka was supported by surface drifters during the summer months (Molinari *et al.,* 1990). No transport value was given for the undercurrent. The equatorward component of the upwelling-favorable wind along the west coast strengthens in April, reaches a maximum in August and weakens in October. This behavior led Shetye *et al.* (1990) to conclude that the currents were forced by the local winds. Contrary, McCreary *et al.* (1993) concluded from results of a 2.5 layer model that remote-forcing by the Bay-of-Bengal winds also contributes to their development. In a model sensitivity study with no wind stress in the Arabian Sea, the model still produced a shallow upper layer off southwest India, although weaker than with windstress in the Arabian Sea.

Due to the changing monsoon winds, the changing flow field of the Arabian Sea is of great interest for the understanding of the ocean and its response to the wind. Because of the difficulties in determining an appropriate level of no motion in the Arabian Sea, it is important to support geostrophic transport estimates by direct current observations. So far, no informations for the flow field off southwestern India existed from direct velocity profiles and no transports were given for the coastal undercurrent during southwest monsoon. In this investigation we will combine direct and geostrophic computations obtained during a cruise of RV *Sonne* during August 1993 (hereafter So89) to describe the current field and associated transports off the

southwest coast of India during the southwest monsoon. The observations will be compared to earlier reported results.

2. Instruments and data

During So89 a 150 kHz ADCP was mounted in the hydrographic well for continuous measurements of the near surface flow with a range of about 400 m over deep water. Besides the usual misalignment between the ADCP transducer head and the ships axis the gyro input showed a drift of the order of 0.5° per day. Both effects were corrected by applying a time-dependent calibration with a remaining uncertainty of the order 0.1°. Position data from the Global Positioning System (GPS) were used to transform the relative velocities into absolute currents. The calibrated data were interpolated to a regular grid of 10 m vertically and 0.1° (10 km) horizontally using a Gaussian weighting function. Uncertainties in the shipboard ADCP data were estimated at 5 cm s^{-1}, arising from GPS errors and residual heading bias (order 1 cm s^{-1} at 6 m s^{-1} ship speed). While GPS errors can be reduced by averaging, a heading bias of 1 cm s^{-1} will result in a transport bias of 0.3 Sv per 100 km ship track and 300 m vertical integration. For the approximately 900 km long section from 76°52′E out to 68E such an error could add up to 3 Sv.

The uppermost reliable depth cell of the shipboard ADCP was 24 to 32 m, thereby missing a large fraction of the near surface shear. However, the ship drift determined from the ships Doppler log and GPS navigation was of good quality and visual inspection of the ADCP profiles showed that upward shear extrapolation would match the ship drift (at 10 m depth) in most places. Therefore we introduced ship drift as the top depth cell into the ADCP data set.

In addition to the shipboard ADCP direct observations of the deeper velocity field were obtained by lowering an ADCP (LADCP) with the CTD (Fischer and Visbeck, 1993). On all stations east of 70E a 'broad band' ADCP (BB-ADCP) was used while to the west a 'narrow band' ADCP (NB-ADCP) was used. Unfortunately, the internal compass of the NB-ADCP was mounted 180° off. To first order this was compensated by rotating the currents by that amount. However, there might be deviations of a few degrees arising from the internal compass compensation table applied to the wrong directions. The estimated error of the BB-ADCP is of the order of 5 cm s^{-1} while that of the NB-ADCP might be a little larger. At the four stations nearest to the coast and at 75°45′E no LADCP profiles were gained (Fig. 1). At all other CTD-stations the LADCP was operational.

For the hydrographic profiles a Neil-Brown Mark III system was used. The calibration of the CTD data resulted in accuracies of 0.002°C in temperature, 0.003 in salinity, 4.5 dbar in pressure and 0.07 ml l^{-1} in oxygen. The CTD data were used to calculate geostrophic velocities and transports. As the geostrophic computations show doubtful velocity profiles for stations with small station spacing, the geostrophic velocity distribution was plotted using every second profile near the Indian coast.

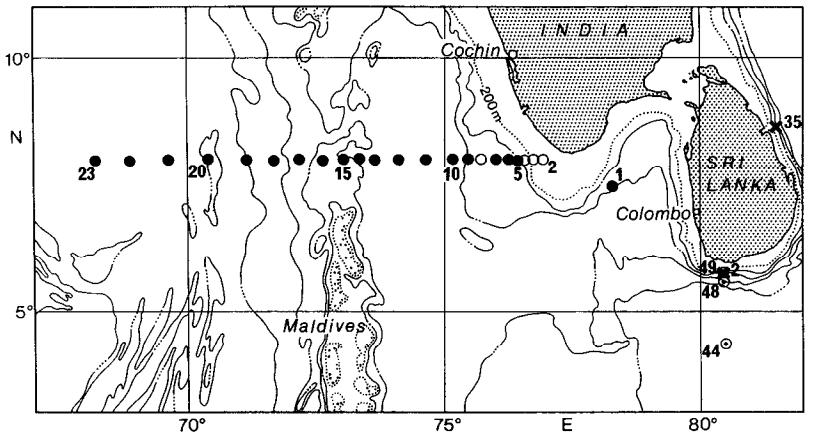

Figure 1. CTD stations (open circles) with station numbers and CTD with lowered ADCP (LADCP) stations (dots) off the southwest coast of India during So89 in August 1993. In addition, some selected stations of RV *Sonne* cruise 88 in July 1993 (open circles with dot) and of *Sonne* cruise 93 in January 1994 (crosses) from south and east of Sri Lanka are used in this analysis. Also shown are the depth contours in 1000 m intervals as well as the 200 m depth contour (dotted).

Using alternatively the stations left out or all stations near the coast would lead to different velocity structures, but the total transport does not change as these stations are located between the corner stations used for the geostrophic transport computations.

The locations of the CTD stations along 8N off the southwest coast of India to 68°10′E from So89 in August 1993 are shown in Figure 1. The section was completed within 4 days (August 5 to August 8, 1993). A first test station (station 1) was carried out southeast of India at 7°30′N 78°15′E and will be used for the water mass investigation. The CTD section along 8N began on the Indian shelf at 76°52′E. The section was carried out to the west crossing the Chagos-Laccadive Ridge at about 72°50′E. On this ridge the Laccadives are located to the north and the Maldives to the south of the section. The westernmost station of the section used here is located at 68°10′E (Fig. 1). To the west of this station, CTD's were taken but the LADCP was not used.

Additional data from south and east of Sri Lanka were used for supplementing the water mass investigations. These data were taken during RV *Sonne* cruise 88 in July 1993 and *Sonne* cruise 93 in January 1994 and locations of stations selected for this paper are also shown in Figure 1.

Meteorological observations were collected during the entire cruise. The wind velocity along the ship track for each tenth of a degree and surface currents determined from the ship drift measurements are presented in Figure 2. The wind distribution (Fig. 2 top) shows the southeastward monsoon component along the

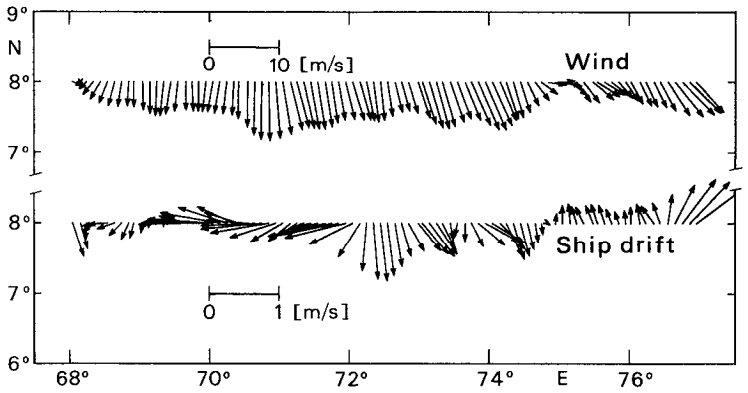

Figure 2. Wind observations in m/s (3 hours low pass filtered) (top) and ship-drift from the ship-navigation system in m/s^{-1} (5 hours low pass filtered) (bottom), at 0.1° longitude resolution along 8N, August 5 to August 8, 1993.

section. The ship drift at some locations deviated from the wind direction indicating that the surface flow is governed by the currents and not the Ekman flow.

3. The water masses

The upper ocean water masses off the southwest coast of India are characterized by Indian Equatorial Water (IEW, Sverdrup *et al.,* 1942; Emery and Meincke, 1986), with possible intrusions of more saline Arabian Sea Water (ASW) or less saline Bay of Bengal Water (BBW). Using hydrographic and sea level data, Banse (1968) concluded that cool upwelled water is present on the shelf off the southwest coast of India during the southwest monsoon and the upwelling causes an uplift of the 20°C isotherm by 90–100 m. According to Darbyshire (1967) the northward flow during November to January carries low density Equatorial Surface Water to the north. Associated with this flow is a downdraft of ASW and a depression of the thermocline down to about 100 m depth. In May to early September there is a retreat of Equatorial Surface Water and an upward movement of Arabian Sea Water.

Underneath the surface water is a water mass called Red Sea Persian Gulf Intermediate Water by Emery and Meincke (1986) or North Indian Intermediate Water by Wyrtki (1973). This water mass can be identified by a salinity maximum at about 300 m depth from the Persian Gulf usually found only north of 10N and a deeper salinity maximum at 500 to 800 m depth (Wyrtki, 1971) originating from the Red Sea and an oxygen minimum just underneath. Therefore, this water mass receives the characteristics from two different sources and is sometimes treated independently as Red Sea Water or Persian Gulf Water, respectively. Near-zero concentrations of oxygen in the North Indian Intermediate Water is maintained by moderate consumption applied to waters with initially low oxygen concentrations that pass through the layer at moderate speed (Swallow, 1984; Olson *et al.,* 1993).

This layer extends from above 200 m to more than 1200 m depth in the Arabian Sea, and has oxygen contents of less than 1 ml l^{-1} everywhere north of 3N (Wyrtki, 1973). The deep water underneath shows very little variability in its Θ-S characteristic. Warren (1993) described the layer between 1500 and 3500 m as North Indian Deep Water spreading southwestward near East Africa driven by the upwelling of bottom water from below.

The hydrographic parameter distribution in August 1993 in the upper 200 m between 68°10′E and the Indian shelf is shown in Figure 3. On the western side of the section the saline, warm and oxygen-rich ASW can be seen. The depth of the 20°C isotherm decreases toward the coast by about 70 m. As expected for the southwest monsoon season the thermocline shallows near the coast. The mixed-layer depth from the temperature distribution is shallower than 60 m east of 72°20′E and shallower than 80 m east of 69°40′E. Due to the northward subsurface flow near the shelf the isotherm depths increases toward the shelf below 80 m. Above 80 m depth the isotherms uplift toward the surface indicating coastal upwelling. Just underneath the mixed layer the water masses show low dissolved oxygen concentrations (Fig. 3c) which rise toward the shelf together with the mixed layer.

The T-S diagram shows that water masses east of 75E mainly consist of IEW with some admixture of ASW (Fig. 4a, solid lines). Water with the characteristics of the low salinity water of BBW (salinity < 35.0) is located at 8N near the surface between 74°20′E and the Indian shelf (Fig. 3b). An alternate explanation of the low salinity water could be an inflow of freshwater from the rivers and backwaters as described by Darbyshire (1967) for the end of the summer monsoon season. The possible flow of BBW around the southern tip of India cannot be confirmed by station 1 at 7°30′N, 78°15′E (dotted line on the left side in Fig. 4a) of this survey as the surface profile of that station shows no strong salinity decrease near the surface. A CTD section along 80°30′E was carried out during RV *Sonne* cruise 88 south of Sri Lanka at the end of July 1993, a few days before So89 began. This data set reveals that the eastward-directed Monsoon Current was separated from the coast by a 60 km wide branch of westward flow, which was identifiable as BBW by its low salinities (Schott *et al.*, 1994). The low salinity water at 8N is found mainly in the region of northward ship drift (Fig. 2 bottom) but was also found at the western side of the section in a region of southward surface currents.

From So89 data alone it is not possible to prove that the low salinity water is BBW, but the observations by Schott *et al.* (1994) indicate a likely connection from the Bay of Bengal around the southern tip of Sri Lanka to the Indian coast in summer 1993. The T-S curves from just south of Sri Lanka in July 1993 (dashed lines at the low salinity side of Fig. 4b) and off India at 8N (solid lines in Fig. 4b) are very similar except that the surface salinities at 8N, probably influenced by rain or river inflow, were lower than south of Sri Lanka. Stations from a later cruise of RV *Sonne* (So93)

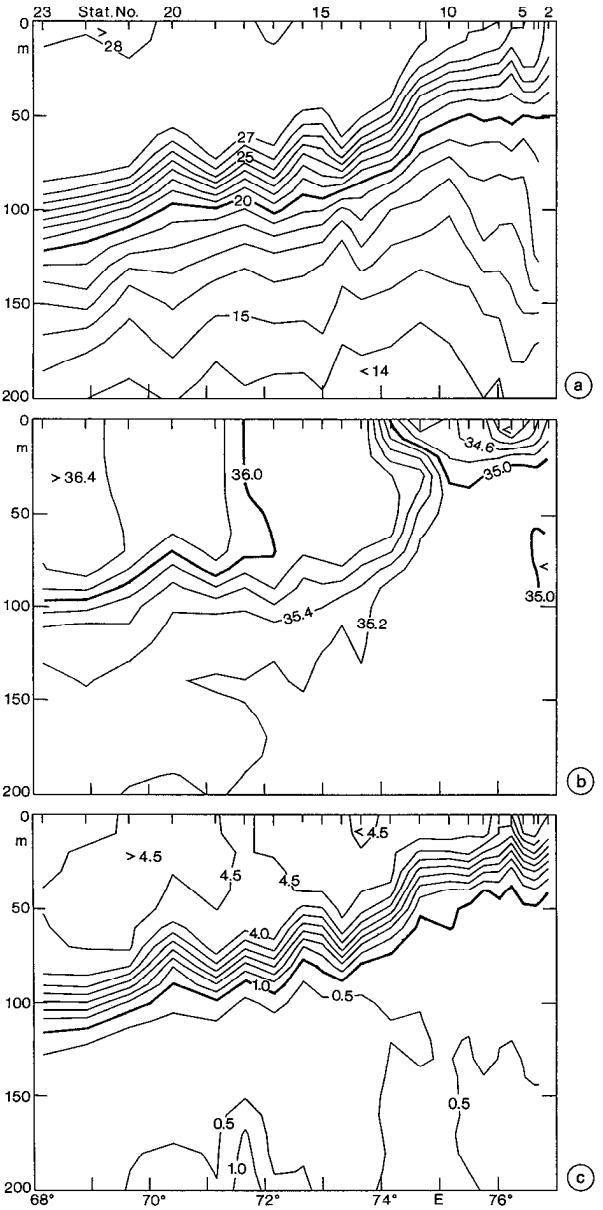

Figure 3. Distribution along 8N for the top 200 m between 68°10′E and the South Indian shelf in August 1993 slightly smoothed with a two-dimensional Gaussian filter for (a) temperature in °C, (b) salinity and (c) dissolved oxygen in ml l^{-1}.

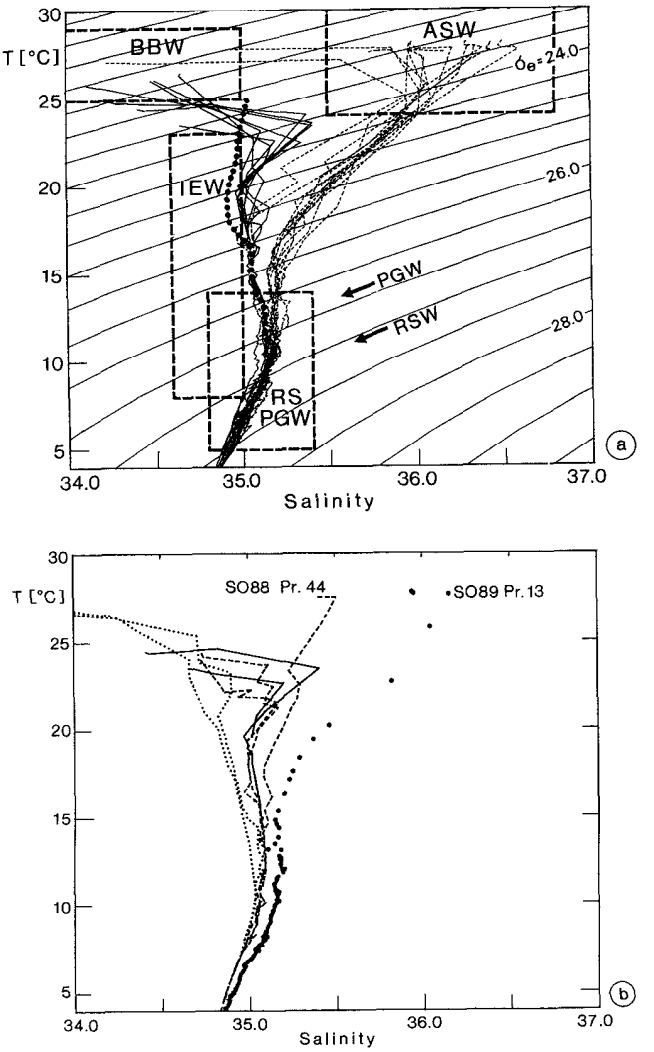

Figure 4. *T-S* distribution (a) for all So89 CTD-stations with stations west of 75E as dashed lines, east of 75E as solid lines and station 1 southeast of India as a dotted line with isopycnals included and (b) for a selection of stations located within Bay of Bengal Water (BBW) from the RV *Sonne* cruises in July 1993 (dashed line), August 1993 (solid line) and January 1994 (dotted line) and one station in August 1993 outside the Bay of Bengal Water at 8N 73°40′E (dots) for comparison (for station locations see Fig. 1). Boxes in (a) show the *T-S* range for Bay of Bengal Water (BBW), Arabian Sea Water (ASW), Indian Equatorial Water (IEW) and Red Sea Pergian Gulf Intermediate Water (RSPGW) with boundaries according to Emery and Meincke (1986) and the density surfaces of the core of Persian Gulf Water (PGW) and Red Sea Water (RSW) marked by an arrow.

in January 1994 south and east of Sri Lanka (dotted lines in Fig. 4b) show *T-S* characteristics similar to those in August 1993 except that the salinity was even a little lower in January. As the January profiles come from the northeast monsoon period the close similarity of the January profiles south and east of Sri Lanka with the profiles near the Kerala coast gives strong evidence that Bay of Bengal Water was found off southwest India in August 1993. For comparison one station of the southward flow along 8N (dots) and one station south of Sri Lanka located in the eastward Monsoon Current (dashed line at the high salinity side of Fig. 4b) are presented and show that the water mass characteristics outside the possible flow route of BBW is different.

The presence of BBW off India at 8N near the surface was somewhat unexpected, as during June-August 1987 Shetye *et al.* (1990) observed near-surface salinities in the range 35.0 to 36.5 on several sections perpendicular to the Indian coast between about 8N and 22N; i.e. much higher salinities than in August 1993 and outside the salinity range of BBW. Instead, Shetye *et al.* (1990) found water with salinities below 35.0 at temperatures between 14°C and 20°C in the coastal undercurrent, which they called BBW because of the close similarity to a mean profile in the southwestern Bay of Bengal (80–85E, 5–10N) below 20°C. But compared to the water mass definitions by Emery and Meincke (1986) used here, this water falls into the range of IEW. Our profile in January 1994 off the northeast coast of Sri Lanka (Fig. 4b) showed lower salinities than west of India below 20°C, not reproducing the similarity found by Shetye *et al.* (1990).

At station 1 southeast of India (dotted line in Fig. 4a) the upper ocean shows a clearer signal of IEW than at the 8N section. The splitting of the *T-S* curves at 8N into water influenced by IEW and water influenced by ASW appears to be located at temperatures above 13°C corresponding to depths shallower than 250 m. The smallest variability along 8N in the RSPGW is observed at about 9°C or about 600 m depths. Above and below that depth the *T-S* curves show larger variability, and a weak salinity maximum appears at about 10.5°C or 500 m depth. The density of σ_Θ = 27.0 at the salinity maximum is in between the core layer density of Red Sea Water in the Gulf of Aden of σ_Θ = 27.25 and Persian Gulf Water of σ_Θ = 26.7 (Quadfasel and Schott, 1982). Wyrtki (1971) determined the depth for Red Sea Water at about 570 m at 8N and at 280 m for Persian Gulf Water. Therefore the salinity maximum near 500 m seems to be caused mainly by water from the Red Sea.

4. Currents and transports

a. Shipboard ADCP. The velocity distribution in the upper ocean from the shipboard ADCP in August 1993 is presented in Figure 5 for the east and north components. Northward velocity is found between 75°20′E and the Indian shelf at 77E restricted mainly to the upper 200 m. Velocities up to 25 cm s^{-1} were observed in a subsurface

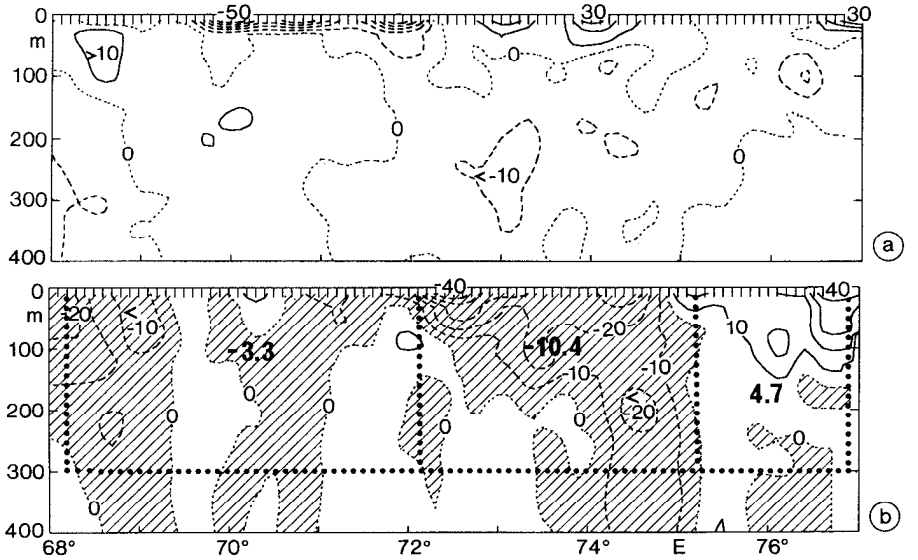

Figure 5. Shipboard ADCP velocity (with ship drift used for the top depth cell) in cm s^{-1} in August 1993 for (a) the zonal component and (b) the meridional component (southward is shaded) at 8N between 68E and the Indian shelf at 76°20′E. Contour interval is 10 cm s^{-1}. Transports in Sv (b) within boxes indicated by dots.

core at about 100 m depth near 76E while above this subsurface core the northward velocity is reduced to 10 to 15 cm s^{-1}. At the eastern side near 77E near-surface velocities of 40 cm s^{-1} are present which are measured by ship drift used for extrapolating the shipboard ADCP toward the surface. Southward flow is found in most places between 68°10′E and 75°20′E, but the velocities are confined to the near-surface layer. Larger southward flow extending below 200 m depth is observed only between 74E and 75E (Fig. 5b) and between 68°10′E and 69°20′E. The highest southward surface velocity is observed at 72°30′E on the western side of the Chagos-Laccadive Ridge (centered at about 72°50′E) with velocities of up to 50 cm s^{-1}. In the central Arabian Sea, further west of the Chagos-Laccadive Ridge, currents were generally weak. Only at the western end of the section from 68°10′E to 69°20′E southward velocities of 10 cm s^{-1} to 20 cm s^{-1} are found in the upper 100 m. The zonal component (Fig. 5a) was mainly westward between 100 and 300 m east of the Chagos-Laccadive Ridge and eastward west of about 71E.

Three meridional current branches are present and are marked by boxes in the figures (5 to 7). The northward transport near the shelf associated with the poleward undercurrent and integrated over the top 300 m was 4.7 Sv (Table 1). To the west the transport becomes negative and the total 0–300 m transport from the shipboard ADCP west of the undercurrent out to 68°10′E reaches 13.7 Sv. Between the western side of the Chagos-Laccadive Ridge from 72°10′E to 75°E is the regime of the

Table 1. Meridional transports in Sv from shipboard ADCP (with ship drift as top depth cell), lowered-ADCP, geostrophic transports (relative to 1000 dbar) with Ekman component in brackets at 8N for the northward flow at 8N between the shelf (76°25′E for LADCP, 76°52′E for shipboard ADCP and geostrophy) and the flow reversal to southward flow at about 75E.

Depth layer	Shipboard ADCP	Lowered ADCP	Geostrophy (Ekman)
0–100 m	3.5	1.1	2.7 (−0.2)
100–200 m	1.1	0.8	1.4
200–300 m	0.2	0.5	0.0
300–400 m	−0.1	0.3	−0.5
400–500 m	—	0.2	−0.7
0–300 m	4.7	2.4	4.1 (−0.2)

southward flow with a 0–300 m transport of 10.4 Sv. As the *T-S* relation is different for the northward flow (solid lines in Fig. 4a) compared to that of the southward current branches (dashed lines in Fig. 4a), it is evident that the southward flow is not a return flow of the near-coastal northward current. West of the ridge is a region of weak southward flow. In the ship drift data between 69°20′E and 72°10′E the surface flow is mainly westward. Only at 68°10′E to 69°20′E the third current band of a southward flow can be identified with a 0–300 m transport of 3.3 Sv. This current band shows the same *T-S* characteristics as the southward flow east of 72°10′E.

b. Lowered ADCP. In addition to the shipboard ADCP measurements, a lowered ADCP was used during August 1993 to measure the velocity field at 8N shown in Figure 6 for the east and north components. A comparison of the LADCP measurements to the shipboard ADCP currents shows the same directions and velocity features in many regions. But there are regions where both direct methods differ, mainly in the central and western part of the section, some of which could be explained by the lack of near-surface measurements of the LADCP which had the first reliable measurement in about 40 m depth and lower horizontal resolution. For transport calculations we used shear extrapolation toward the surface.

The LADCP transport values for the coastal poleward undercurrent in Table 1 are lower than the values derived from the shipboard ADCP. This is caused by the fact that the easternmost LADCP station was located at 76°25′E while the shipboard ADCP section reached further east. Transports integrated over the same longitude range differ by only 0.2 Sv which is well inside the uncertainties of the measurements. For the two southward current branches the transport differences were larger, at 4 Sv and 2 Sv (Table 2).

c. Geostrophic computations. From the direct current observations close to the continental shelf at 8N a level of no motion is hard to detect. At depths greater than

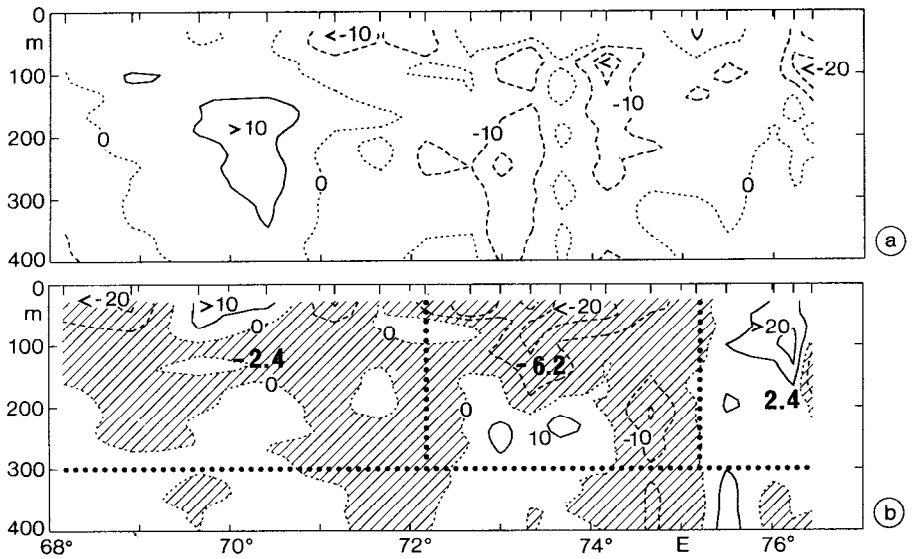

Figure 6. Velocity in cm s^{-1} for (a) the zonal component and (b) the meridional component (southward is shaded) at 8N in August 1993 from the lowered-ADCP. Contour interval is 10 cm s^{-1}. Transports in Sv (b) within boxes indicated by dots.

600 m the LADCP shows small meridional velocities at most locations. A possible level of low vertical shear and small horizontal variability is found roughly between 900 m and 1000 m in the LADCP profiles, confirming that the choice of a level of no motion at 1000 m was reasonable.

Table 2. Meridional transport in Sv from shipboard ADCP (with ship drift as top depth cell), lowered-ADCP, geostrophic transports (relative to 1000 dbar) with Ekman component in brackets for the southward flow at 8N (a) between the western side of the northward undercurrent at about 75E and 72°10′E and (b) between 72°10′E and 68°10′E.

(a) Depth layer	Shipboard ADCP	Lowered ADCP	Geostrophy (Ekman)
0–100 m	−6.6	−4.3	−3.7 (−0.3)
100–300 m	−3.8	−1.9	−1.0
300–500 m	—	0.2	−0.5
500–1000 m	—	−1.6	−1.2
0–300 m	−10.4	−6.2	−4.7 (−0.3)

(b) Depth layer	Shipboard ADCP	Lowered ADCP	Geostrophy (Ekman)
0–100 m	−2.1	−1.5	−2.3 (−0.2)
100–300 m	−1.2	−0.9	−0.6
300–500 m	—	0.7	−0.2
500–1000 m	—	1.8	−0.6
0–300 m	−3.3	−2.4	−2.9 (−0.2)

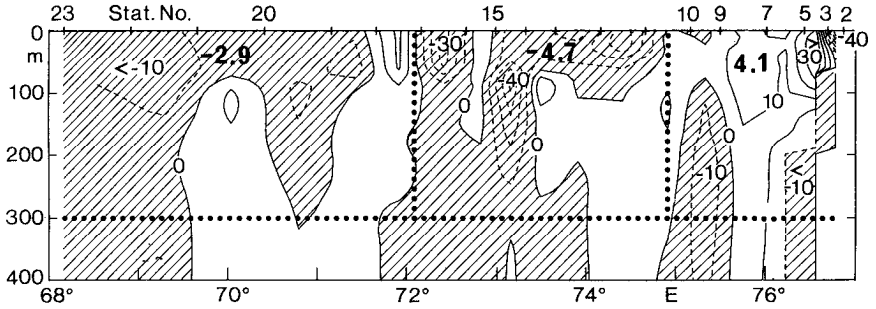

Figure 7. Geostrophic currents during So89, August 1993, relative to 1000 dbar across 8N in cm s^{-1} (southward is shaded). Transports in Sv within boxes indicated by dots.

For geostrophic computations a reference depth has to be determined. In the Atlantic Ocean, the boundaries between water masses spreading into different directions can be used as levels of slow motion. In the Arabian Sea the deeper water masses are moving slowly, water masses are difficult to separate, and hence the water mass distribution is of little help for the choice of a reference depth. Shetye *et al.* (1990) computed the geostrophic transport relative to 1000 dbar. Here, based on the evidence from the direct observations, geostrophic computations were also carried out relative to 1000 dbar to compare the transport values to the estimates of the direct measurements. Figure 7 shows the geostrophic velocity of the upper ocean across the 8N section which should be compared to the north components from the shipboard and lowered ADCP (Figs. 5b and 6b).

In the upper 400 m (Fig. 7) the general structure is similar to the shipboard ADCP distribution. The geostrophic field also reveals the three meridional current bands. In the central Arabian Sea the southward flow is located between 68°10′E and 69°30′E and maximum velocities of up to 15 cm s^{-1} are found. Geostrophic calculations from the CTD-stations to the west of 68°10′E showed that the current band started at 66E and had its largest velocities at 67E, i.e., this current band is not completely covered by the section used. The geostrophic transport for the current band east of 68°10′E is −2.9 Sv for the upper 300 m (Table 2b) while the geostrophic transport (0–300 m) between 66°40′E and 68°10′E is −4.3 Sv. This leads to a total 0–300 m geostrophic transport of −7.2 Sv for the westernmost current band.

On the eastern side of the Chagos-Laccadive Ridge there is a region between 72E and 74°45′E with strong southward flow of up to 40 cm s^{-1} at 100 m depth. The geostrophic transport in the upper 500 m is −5.2 Sv (Table 2a). Adding −0.3 Sv for the Ekman transport determined from the ship wind measurements yields −5.5 Sv for this band, similar, within the error bars, to the value of −6.0 Sv from the lowered ADCP.

Different from the shipboard ADCP data, the geostrophic northward flow between 75E and 76°40′E shows no clear subsurface core, instead the maximum velocities of up to 30 cm s^{-1} are located near the surface. The different depths of the

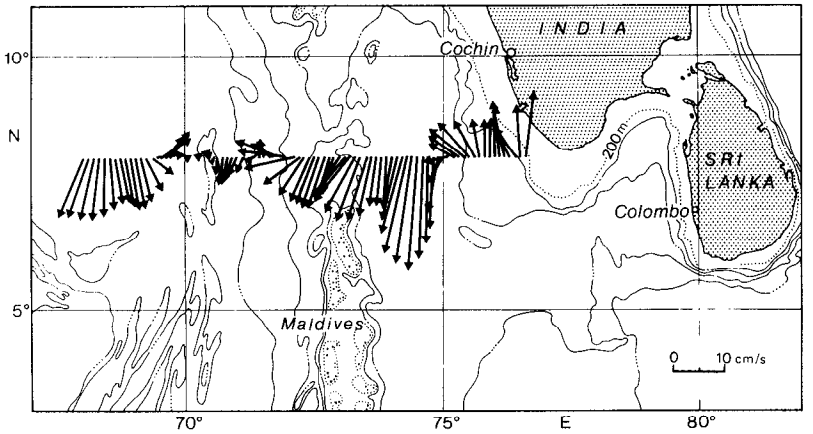

Figure 8. Vertically averaged (0–300 m) currents from shipboard ADCP. Depth contours as listed in Figure 1.

velocity maxima in geostrophy and shipboard ADCP in the upper ocean are probably caused by the Ekman flow, as the southward Ekman flow caused by the surface winds (Fig. 2 top) of 0.2 Sv is included in the ADCP measurements while not included in the geostrophic flow field.

The geostrophic transport supplemented by the Ekman contribution amounted to 3.9 Sv for the near-coastal northward flow for the upper 300 m (Table 1), thereby being 0.8 Sv less than the transport of the shipboard ADCP. However, the 0–400 m geostrophic transport of 2.7 Sv for the northward current band, defined between stations with LADCP available that is offshore of 76°25'E, coincides with that of the LADCP. The major difference in the transport calculation appears on the eastern side near the coast, where the geostrophic velocities turned to weak southward flow at the inshore station pair while the velocity distribution of the shipboard LADCP showed continuous northward flow near the coast.

5. Discussion

Direct velocity measurements and geostrophic computations were used to investigate the flow field and to compute the transports off the southwest coast of India east of 68°10'E at 8N during the southwest monsoon in August 1993. All three methods showed the poleward coastal undercurrent as well as two southward current bands further west, east of 68°10'E, which in Figure 8 are represented by the mean 0–300 m velocity distribution of the shipboard ADCP. Between the northward flow near the coast and the southward flow further offshore, there is no transition zone with weak currents, but the water mass distribution within these two bands is different and the southward flow is not a local recirculation of the northward flow or an eddy-like

feature. The transport calculations for the deeper layers (Table 1, 2) show that the major contribution is from the upper 300 m.

The northward undercurrent hugging the continental slope, which was described earlier by Shetye *et al.* (1990), was observed here with a transport of 4.7 Sv in the upper 300 m from the shipboard ADCP. Different from the result of a southward geostrophic surface flow above the undercurrent (Shetye *et al.,* 1990) the northward flow in August 1993 extended toward the surface. Mean ship drift data for July (e.g. McCreary *et al.,* 1993) and August (e.g. Shetye *et al.,* 1993) show a clear southward flow at the surface. A southward surface flow would indicate a typical eastern boundary upwelling region where an equatorward wind generates equatorward surface flow and upwelling. The undercurrent's existence in model simulations strongly depends on the existence of an alongshore pressure gradient caused by the meridional wind field distribution (Clarke, 1989). Only if there is a positive wind curl near the coast, model results reach commonly observed undercurrent velocities (McCreary and Chao, 1985). While Shetye *et al.* (1990) conclude that the upwelling along the coast is controlled by the local winds, McCreary *et al.* (1993) demonstrate that remote forcing due to winds in the Bay of Bengal and south of India is influencing the west-coast upwelling via the northward propagation of the raised thermocline along the west coast of India as a package of Kelvin waves. From our observations of weaker than normal winds off southwest India (see below) and the flow of Bay of Bengal Water within the undercurrent, our data support the findings of McCreary *et al.* (1993) of remote forcing due to the winds in the Bay of Bengal.

The water mass distribution in the upper ocean off India at the eastern end of the 8N section shows Arabian Sea Water offshore in the regime of southward flow while east of 75E the *T-S* characteristics indicate a large contribution of Indian Equatorial Water to the northward-flowing undercurrent. In the region of the southward flow west of 75E the mixed layer depths increased to 60 m at about 72°20′E and to 80 m at about 69°40′E. From model results with a 2.5 layer model McCreary *et al.* (1993) found that shallow mixed-layer depths are not trapped at the coast, but propagate westward throughout the year with a considerably faster speed in the south than in the north.

The direct observations show a clear subsurface core of the northward current near the Indian shelf. This subsurface core is not as well developed in the geostrophic velocity distribution as in the direct observations. From the ships wind observations a southward contribution of −0.2 Sv (Table 1) from the Ekman flow was computed for the width of the northward flow. As the direct observations include the Ekman component while the geostrophic method does not, the difference in the velocity distribution near the surface might be explained by the Ekman component. In the region of southward flow at the western side of the section the velocities in the upper 100 m are larger from the shipboard ADCP than from geostrophy. Here the currents

and the Ekman flow were in the same direction and the ADCP is expected to measure the larger velocities.

The observed wind during the cruise (Fig. 2 top) shows weaker wind velocities between 74°30′E and 76°30′E than the typical long-term mean for August. According to the maps by Hastenrath and Lamb (1979), the long-term mean August wind for this region should be southeastward with 4 to 5 m s^{-1}. At the same location the surface currents observed in August 1993 were northward, opposite to the long term ship drift of Cutler and Swallow (1984) showing a southeastward flow off the Kerala coast. The westward flow just south of Sri Lanka (Schott *et al.,* 1994) seemed to be also connected to weaker winds. The observed wind in this region of westward flow was around 4 to 5 m s^{-1} to the east compared to the long-term mean July/August wind velocity of about 6 m s^{-1} to the east for this area (Hastenrath and Lamb, 1979). The flow of Bay of Bengal Water around the southern tip of Sri Lanka at the end of July 1993 (Schott *et al.,* 1994) and the northward flow of Bay of Bengal Water in the upper 50 m in the near-coastal current band could be related to the weaker wind velocities at that time which opposite to the regular situation seem to allow a northward flow just off the coast. The FSU winds (described by Stricherz *et al.,* 1993) over the Arabian Sea show northwestward directed pseudostress anomalies off the southwest coast of India in June 1993 and northeastward directed anomalies in July 1993. The northward-directed anomaly in the two months prior to the ship cruise supports the assumption that the northward coastal surface current was caused by the wind anomalies.

Two southward current bands were present above and east of the Chagos-Laccadive Ridge and at 68°10′E to 69°20′E (Fig. 8). From geostrophic computations east of 68°10′E it was shown that the westernmost current band continued to the west and only part of it is located in the section used here. The southward flow between 72°10′E and the boundary to the northward undercurrent results in an 0–300 m transport of −6.2 Sv from the lowered ADCP. This is larger than the −4 Sv described by Shetye *et al.* (1990) for the coastal current of 150 km width. The main reason is the larger horizontal extension (280 km wide) of the southward flow, although the deeper reaching part of the current (74E to 75E) was only 100 km wide.

In the region of the near-shore northward current, east of 75E, the ship drift shows a continuous northward component while the wind is directed to the southeast and hence should result in a southward Ekman flow. This indicates that the Ekman flow is not strong enough to erase the northward flow at the surface but only reduces the velocity and in consequence the flow reveals a subsurface velocity maximum. Also the two southward flows between 72°10′E and 75E and with a weaker signal west of 69°20′E are represented in the ship drift data.

In an earlier investigation in the Atlantic, Stramma *et al.* (1995) compared direct and geostrophic transport computations and found similar transports from both methods in a region of a strong current. Here, we showed that this could also be

applied to regions of rather weak currents. Because of the changing flow fields with the monsoon seasons, the transports given here for the Indian Ocean are valid only for the August of 1993, but these results can be used for comparison with the transports measured in the future at different times of the year or at the same month in other years. For the first time the transport of the coastal undercurrent was estimated from direct current profiles during southwest monsoon.

Acknowledgments. We thank the captain and crew of the RV *Sonne* for their help, C. Meinke for technical assistance, O. Plähn for doing some of the computations, A. Eisele for drafting the figures and J. Reppin for extracting plots of the FSU data set. D. Quadfasel made the *Sonne* 88 and 93 CTD profiles available to us. We acknowledge financial support for *Sonne* cruise 89 from the German Bundesministerium für Bildung, Wissenschaft, Forschung und Technologie (grant 03R430) and from the German WOCE project (grant 3F01212A).

REFERENCES

Banse, K. 1968. Hydrography of the Arabian Sea shelf of India and Pakistan and effects on demersal fishes. Deep-Sea Res., *15,* 45–79.

Bruce, J. G., D. R. Johnson and J. C. Kindle. 1994. Evidence for eddy formation in the eastern Arabian Sea during the northeast monsoon. J. Geophys. Res., *99,* 7651–7664.

Clarke, A. J. 1989. Theoretical understanding of eastern ocean boundary poleward undercurrents, *in* Poleward Flows Along Eastern Ocean Boundaries, S. J. Neshyba, C. N. K. Mooers, R. L. Smith and R. T. Barber, eds., Coast. Estuar. Stud., *34,* 26–39.

Cutler, A. N. and J. C. Swallow. 1984. Surface currents of the Indian Ocean (to 25°S, 100°E): compiled from historical data archived by the Meteorological Office, Bracknell, U. K. Institute of Oceanographic Sciences, report no. *187,* 8 pp. and 36 charts.

Darbyshire, M. 1967. The surface waters off the coast of Kerala, southwest India. Deep-Sea Res., *14,* 295–320.

Emery, W. J. and J. Meincke. 1986. Global water masses: summary and review. Oceanologica Acta, *9,* 383–391.

Fischer, J. and M. Visbeck. 1993. Deep velocity profiling with self-contained ADCP's. J. Atmos. Ocean. Tech., *10,* 764–773.

Hastenrath, S. and P. J. Lamb. 1979. Climatic atlas of the Indian Ocean, part I: surface climate and atmospheric circulation, University of Wisconsin Press, 93 pp.

McCreary, J. P. Jr. and S.-Y. Chao. 1985. Three-dimensional shelf circulation along an eastern ocean boundary. J. Mar. Res., *43,* 13–36.

McCreary, J. P. Jr., P. K. Kundu and R. L. Molinari. 1993. A numerical investigation of dynamics, thermodynamics and mixed-layer processes in the Indian Ocean. Prog. Oceanogr., *31,* 181–244.

Molinari, R. L., D. Olson and G. Reverdin. 1990. Surface current distributions in the tropical Indian Ocean derived from compilations of surface buoy trajectories. J. Geophys. Res., *95,* 7217–7238.

Naqvi, S. W. A., R. J. Noronha, K. Somasundar and R. Sen Gupta. 1990. Seasonal changes in the denitrification regime of the Arabian Sea. Deep-Sea Res., *37,* 593–611.

Olson, D. B., G. L. Hitchcock, R. A. Fine and B. A. Warren. 1993. Maintenance of the low-oxygen layer in the central Arabian Sea. Deep-Sea Res., *40,* 673–685.

Quadfasel, D. D. and F. Schott. 1982. Water-mass distribution at intermediate layers off the Somali coast during the onset of the southwest monsoon, 1979. J. Phys. Oceanogr., *12,* 1358–1372.

Rao, R. R., R. L. Molinari and J. F. Festa. 1989. Evolution of the climatological near-surface thermal structure of the tropical Indian Ocean: 1. Description of mean monthly mixed layer depth, and sea surface temperature, surface current and surface meteorological fields. J. Geophys. Res., *94,* 10801–10815.

Schott, F., J. Reppin, J. Fischer and D. Quadfasel. 1994. Currents and transports of the Monsoon Current south of Sri Lanka. J. Geophys. Res., *99,* 25127–25141.

Shetye, S. R., A. D. Gouveia, S. S. C. Shenoi, D. Sundar, G. S. Michael, A. M. Almeida and K. Santanam. 1990. Hydrography and circulation off the west coast of India during the southwest monsoon 1987. J. Mar. Res., *48,* 359–378.

Shetye, S. R., A. D. Gouveia, S. S. C. Shenoi, G. S. Michael, D. Sundar, A. M. Almeida and K. Santanam. 1991. The coastal current off western India during the north-east monsoon. Deep-Sea Res., *38,* 1517–1529.

Shetye, S. R., A. D. Gouveia, S. S. C. Shenoi, D. Sundar, G. S. Michael and G. Nampoothiri. 1993. The western boundary current of the seasonal subtropical gyre in the Bay of Bengal. J. Geophys. Res., *98,* 945–954.

Stramma, L., J. Fischer and J. Reppin. 1995. The North Brazil Undercurrent. Deep-Sea Res., *42,* 773–795.

Stricherz, J. N., D. M. Legler and J. J. O'Brien. 1993. Atlas of Florida State University Indian Ocean winds for TOGA 1970–1985. Florida State University, Tallahassee, technical report, 6 pp and plates.

Sverdrup, H. U., M. W. Johnson and R. H. Fleming. 1942. The oceans, their physics, chemistry and general biology, Prentice-Hall, 1060 pp.

Swallow, J. C. 1984. Some aspects of the physical oceanography of the Indian Ocean. Deep-Sea Res., *31,* 639–650.

Warren, B. 1993. Circulation of north Indian deep water in the Arabian Sea. *in* Oceanography of the Indian Ocean, B. N. Desai, ed., Balkema Rotterdam, 575–582.

Wyrtki, K. 1971. Oceanographic atlas of the International Indian Ocean Expedition. National Science Foundation, Washington, D.C., 521 pp.

—— 1973. Physical oceanography of the Indian Ocean, *in* The Biology of the Indian Ocean, B. Zeitzschel and S. A. Gerlach, eds., Chapman and Hall LTD, London, 18–36.

Received: *7 March, 1995;* Revised: *28 August, 1995.*